Compensation of Azimuthal Distortions on a Free Spinning 2D Laser Range Finder for 3D Data Set Generation

R. Pascoal, V. M. Santos, *Member, IEEE*

***Abstract*—Due to several limiting factors of using the currently available 3D laser scanners, including their high cost, an interesting alternative approach is arising among several researchers. That approach consists of taking advantage of 2D laser range finders in dynamic arrangement to generate 3D data. Most 2D laser rangers are based internally on a rotating mirror which deflects a laser beam in several azimuths. This approach is valid if the device is kept static or with small dynamics. However, if more demanding composite motions are imposed to the scanner, namely rotations, the assumptions made by the internal software are not met and measurements will be affected due to the delays in the measuring process. This paper takes into account the composition of internal plus external movements to compensate for those distortions. The range distances are still correct under those conditions, but the raw instantaneous 3D data points are not, namely those on the periphery of the scan with larger azimuths. The number of applications of 3D laser is huge and the results are relevant and applicable in many situations. Physically, the scanning vector draws a rosette shape on the sensor plane and the third dimension is presently achieved through concentric rotation of a 2D industrial grade scanner. The exact shape of the rosette is dictated by the angular velocity of the additional external shaft and it is shown in this paper how this variable can be controlled to achieve the most adequate combination of point density and frame rate. Correction of the scans to account for the external angular velocity is demonstrated.**

I. Introduction

THE use of lasers in guidance and navigation is found in diverse fields, from small mobile robots [1, 2], to aiding huge ships in harbors and canals [3, 4] and warfare [5]. Several applications, such as ship harbor maneuver assistance and missile guidance, use single beam lasers, either to determine distance or to provide a detectable target to be acquired through additional sensors or by humans. Others, such as guidance of industrial robots [6] and most research carried out in obstacle detection and path planning [7], use 2D range finders as means of enabling the detection of surrounding interest objects. These range finders have become quite common also in guidance and navigation of automobiles participating in competitions such as the DARPA Grand Challenge [8] and are commonly complemented by the use of cameras. Only more recently the use of 3D laser scanners has also been equated, but publications still indicate that there are many difficulties related to processing these data [9, 10]. Additionally, though the equipment capable of producing 3D scans is commercially available, they are still very expensive and most are not eye safe nor indicated for navigation, but rather for scene reconstruction.

Several authors have proposed configurations which produce 3D scans based on nodding or rotating existing 2D scanners [11-14]. In all published material, the angular velocity which is imposed on these 2D scanners has been considered low when compared to that of the internal mirror and therefore these have traditionally been considered as a sequence of 2D scans. The fact that they are nodded or rotated at low speed basically reduces applicability to static scenes and when there is very limited ego-motion. These limitations have instigated additional research and development of prototype hardware and software which is reported herein.

II. Prototype Setup

The Laboratory for Automation and Robotics (LAR) at the Department of Mechanical Engineering, University of Aveiro, Portugal, has developed a 3D laser unit with a mechanical setup depicted in Fig. 1.

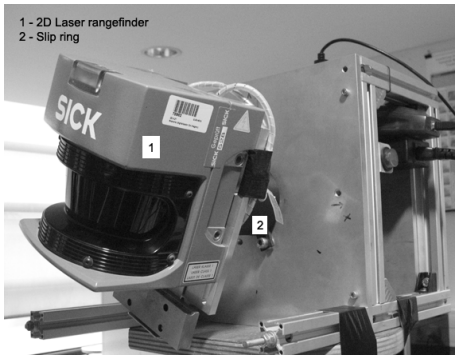

Fig. 1 View of the rotating laser range finder setup at the LAR.

The system is designed to rotate a 2D laser about a shaft which is perpendicular to the scanner's internal mirror axle. The scanner is in forward looking position because it is to be installed onboard a robot with a prevalent sense of motion. To rotate the external shaft, a stepper motor is used with its angular velocity controlled by an MCU. In order to establish connection between the rotating scanner and the fixed part of the platform, a slip ring with adequate signal to noise

Manuscript received 20 January, 2010.

R. Pascoal is currently a visiting researcher at University of Aveiro. The author thanks FCT for funding under BPD/42261/2007 Email: rpascoal@ua.com.

V. Santos is with the Department of Mechanical Engineering and the Centre for Mechanical Technology and Automation of the University of Aveiro. Email: vitor@ua.pt.

ratio and power capability has been installed.

The velocity feedback is achieved through a quadrature encoder which is rigidly connected to the shaft, and velocity commands are sent through a PC interface built around CARMEN and IPC [15-17]. A new module, consisting of a multi-threaded application running under Ubuntu Linux, was developed to subscribe the 2D laser messages available through IPC, to acquire the external shaft position provided through USB by the mentioned MCU, and the combined input data is then followed by adequate processing procedures. Both laser message and position are time-stamped and therefore this is used to deal with the asynchronous nature of the combined data acquisition. Because, in the present configuration, 2D scans are retrieved in a single packet, precision of the time-stamping, at higher external angular velocities, is absolutely necessary to assign the correct external angle to each detected range. Hence, range will have a director vector which is characterized by its spherical coordinates.

With the mentioned setup, there are several interesting features which, to the authors' knowledge, have not been previously exploited for 3D laser scanning in dynamic environments. Probably the most interesting feature is that the controlled shaft velocity allows the choice among the most useful combinations of point density and rate of the 3D scan.

III. Configuration Properties

The proposed configuration possesses non-negligible angular velocity of the external shaft and, therefore, processing of the 3D scene cannot be carried out simply as if it were a sequence of 2D scans. The range vector coordinates need to be corrected for the externally imposed motion. Although, in this case, processing has additional steps, it is not a computational bottleneck since there will always be the need to account for sources of ego-motion such as originated by platform motion and they are necessary for correct perception.

The external angular velocity actually makes the scanners range director vector travel along rosette shaped trajectories, which are indicated for detecting objects without the need for dense scanning. Necessarily, the sensor sacrifices point density in favor of speed, but those objects which traverse the scene scanned by this setup will very likely be detected. Those situations in which detection will not occur are concerned with objects that have spiral type trajectories fitting exactly out of the scanners field of view or speeds and that are not compatible with the scan rate.

The sensor used in this work is a SICK LMS-200, which is a time-of-flight laser range finder. Because precision timing is of utmost importance in this mode of operation, high speed electronics are a major part of the internal hardware, including FPGA and ASIC. Since scanning is still performed by a single laser beam and avalanche photodiode type sensor, this setup also provides a better platform for coexistence of multiple scanners in the same area, or even multiple scanners rotating in the same setup, by reducing the likelihood of undesirable sensor interactions due to simultaneous operation of the active principle.

Data acquired from the prototype, as mentioned, has the particular feature of scanning 3D space with a director vector that draws a rosette shape on a virtual plane perpendicular to the external shaft. The range vector is defined by its spherical coordinates:

$$\vec{r} = r(t)\cdot\left[\cos\theta(t)\cos\phi(t) \quad \cos\theta(t)\sin\phi(t) \quad \sin\theta(t)\right] \quad (1)$$

in which the range, $r(t)$, and the internal mirror angle, $\theta(t)$, are given by the laser unit internal systems. The origin of the reference system is centered at the point where the laser beam leaves the internal mirror. The second component of the range vector is positive up and the third is positive forward. The coordinate system is illustrated in Fig. 2.

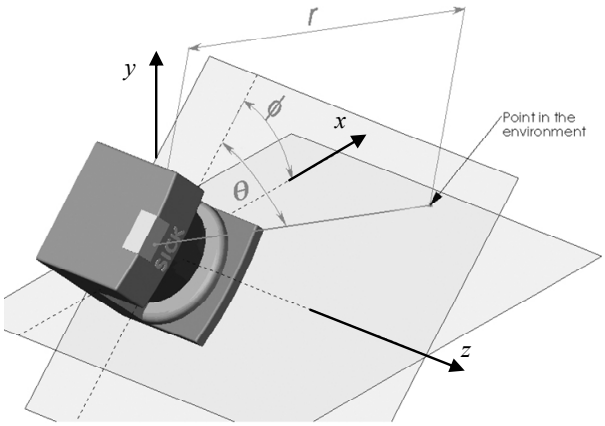

Fig. 2 - 3D measurement coordinates

Range is determined by electronics connected to the laser module and the angle by the reading of an encoder, as shown in Fig. 3.

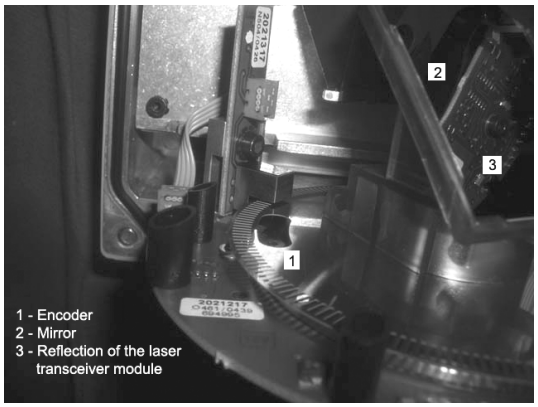

Fig. 3 The internal shaft encoder used to determine the internal mirror angle. Based on image from [18].

The external shaft angle, $\phi(t)$, is measured in real-time by external electronics. The measurements in $\theta(t)$ are equally spaced, therefore their relative time stamp can be assumed to be fixed. The issue is that $\phi(t)$ evolves, asynchronously, but at high data rate, during a full azimuthal laser scan; this

distortion has to be modeled and corrected.

By normalizing the range vector and projecting it onto the sensor plane, the rosettes are found by applying the following expression:

$$\vec{x}_r = \left[\cos\theta(t)\cos\phi(t) \quad \cos\theta(t)\sin\phi(t)\right], \qquad (2)$$

An example of the incomplete rosettes as calculated using equation (2) is shown in Fig. 4.

The thin straight lines in Fig. 4 are those that would be scanned by the ranger if it were to have fictitious instantaneous snapshot capability triggered at the exact instant that a new real scan begins. At 40 Hz the thin lines would actually be scanned twice, once in one direction and a second time in the opposite direction. A single scan is plotted in Fig. 5 for clarifying the relation between scan and its respective real scan line. Notice how the snapshot capability would produce a single straight segment, with origin at the initial time instant of the simulated distorted scan, and how they can only meet again at the origin, when the internal angle reaches $\pi/2$.

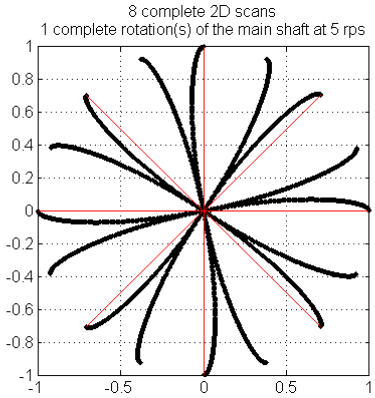

Fig. 4 Sample of trajectory drawn by the director vector on a plane perpendicular to the external axis and located 1 m ahead of the scanner mirror. Case when the 2D scan is at 40 Hz and the external shaft speed is 5 rps.

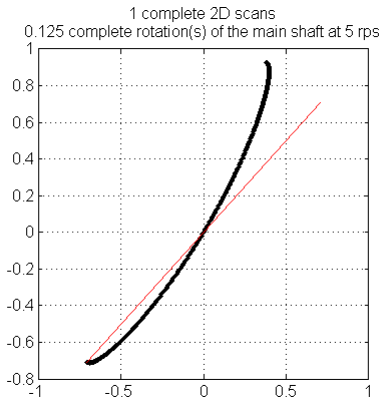

Fig. 5 Sample single scan drawn by the projection of the director vector. Case when the 2D scan is at 40 Hz and the external shaft speed is 5 rps.

The rosettes are incomplete, actually half rosettes, because the particular 2D scanner performs useful scanning only on a 180º sector and thus the time it spends on the blind 180º cannot be plotted. Rosette scanning of domains is found in several sensing applications where computational complexity must be reduced by criterions sampling, such as magnetic resonance imaging and missile target acquisition [19-22].

In applications with rosette scanning by initial design, such as those presented in [5, 21, 22], mostly based on the Risley prism principle [5], it is possible to change the rosette apertures by having control over the two angular velocities. It is easier to focus around points on a particular range, but such is not possible when using standard 2D scanners and thus a less effective focusing mechanism must rely on changing the external shaft speed. On Fig. 6, the effect of changing angular rate to a non-integer multiple of the 2D scanning rate, in this case 7 rps, is demonstrated for a single shaft rotation.

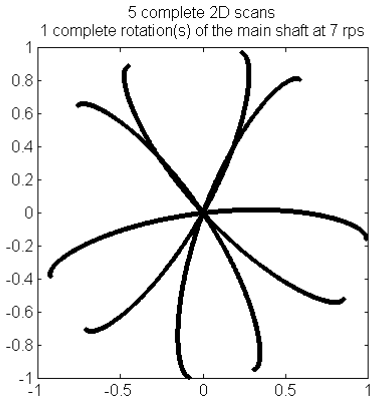

Fig. 6 Sample of trajectory drawn by the director vector on a plane perpendicular to the external axis and located 1 m ahead of the scanner mirror. Case when the 2D scan is at 40 Hz and the external shaft speed is 7 rps.

On Fig. 7 is the same angular rate for a single 2D scan and with the thin line indicating the situation if the scan were instantaneous and it demonstrates that the trajectory is more deformed. On Fig. 8 is the same situation after 3 complete shaft rotations and it demonstrates how the density of the scans increases when external angular is chosen with that criterion in mind.

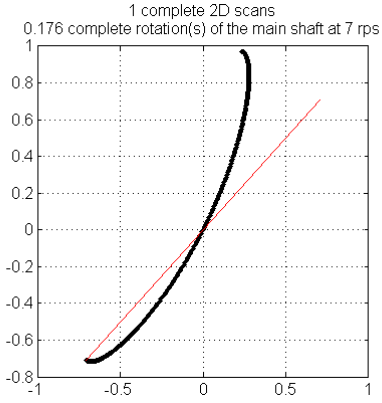

Fig. 7 Sample single scan drawn by the projection of the director vector. Case when the 2D scan is at 40 Hz and the external shaft speed is 7 rps.

During data acquisition, an IPC process is running and messages are passed between the 2D laser scanner module and a 3D laser module which also interfaces with an MCU reading the encoder connected to the external shaft. The 2D

laser scan is time-stamped and this time-stamp is applied immediately after a scan packet starts being received. There is some uncertainty on the exact moment that the internal electronics provide the packet for reading, and this requires further study.

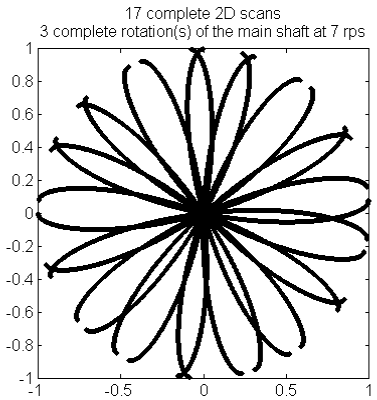

Fig. 8 Sample of trajectories drawn by the director vector on a plane perpendicular to the external axis and located 1 m ahead of the scanner mirror and after three complete shaft rotations. Case when the 2D scan is at 40 Hz and the external shaft speed is 7 rps.

The MCU's main task is to keep track of the encoder position and free time is dedicated to publishing this value, which it manages to perform at a high rate. This value is read by a single thread in the parent process and time-stamped immediately after reading, with several values being kept in memory to enable interpolation. The 2D values are first acquired by internal electronics and are evenly sampled and the angular velocity of the internal stepper motor is also controlled internally.

Because both serial interfaces have hardware buffers, so there remains some uncertainty in the exact time at which data was acquired. This uncertainty is reduced as long as the threads can keep up with the sensor throughput. To eliminate problems resulting from buffer underflow, the threaded serial port reading is blocking and therefore it will stop the thread from running until data is available.

The proposed correction is very simple at this time and consists in the following assumptions. The scanner is externally rotated at a constant angular velocity and it is assumed that the internal mirror is controlled so that it is capable of keeping a constant angular velocity. The effect of Coriolis forces are assumed negligible, but this depends on mirror stability and is not known to be true in practice. In case the assumptions hold, we have an estimated correction of the form:

$$\phi(t_k) \cong \phi(t_0) - \gamma \frac{\Delta\theta_m \times k}{\omega}, k = \{0,1,...,360\} \quad (2)$$

because it is known that each 2D scan is produced at around 37.5 Hz [23], the value of ω is 13320 º/s and the value of $\Delta\theta_m$ is the scan angular interval, selected to be 0.5º. The external shaft angular velocity is γ and is controlled by the MCU. The initial value of $\phi(t_0)$ is considered to be the one obtained by interpolation or extrapolation immediately after a complete scan of the range finder.

IV. Preliminary Experimental Results and Analysis

In order to verify the validity of the proposed correction, an experiment has been setup. The setup consists of having part of a plane ceiling scanned by the prototype at a vertical distance of around y = 1.04 m in the near-field and with the external rotation shaft parallel to the mentioned plane. This is shown in Fig. 8 and allows the calculation of simple statistics and for a conclusion to be drawn about the validity of the proposed correction.

Fig. 9 Experimental setup with leveled range finder scanning the ceiling.

Two situations have been tested, one at close range and a second one at medium range; the close range consists of the patch between 0 m and 4 m from the scanner by two meters wide (centered on the external shaft), and the far range is the patch between 10 m and 14 m by two meters wide and for each of these patches a local average distance is calculated. Because the sparsity of data at high speeds would not provide reasonable statistical confidence without very long runs, the external angular rate has been kept at 1.5 rps. Additional work is also necessary to decouple the MCU and encoder power supply from that of the power electronics (to reduce the effects of current surges due to stepper motor) for correct operation at higher speeds.

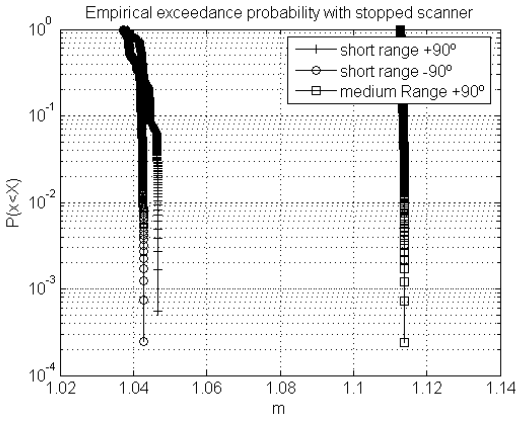

Fig. 10 Empirical exceedance distribution of distance when scanner is *not rotating*.

Fig. 10 to Fig. 12 show the set of empirical cumulative exceedance distribution for real data, collected using the mentioned setup. These distributions are for the local average and have been estimated from sets of about 2000

samples. The cumulative exceedance distribution is defined as the probability that a random variable exceeds a given level, i.e. the probability of exceeding the minimum of a set is 1 and for the maximum the probability is estimated as the inverse of the size of the set.

Fig. 10 shows the empirical distribution for data from the scanner at fixed position; ideally, the empirical distribution would reduce to a vertical line, which would be the exact distance from the scanner to the ceiling (roughly 1.04 m), but with real data there is still some dispersion. Table I shows some summary statistics for data plotted in this figure and there is about 5 mm of error amplitude in the first case.

TABLE I
ERRORS FOR SCANNER AT A FIXED POSITION

statistic/angle	+90 º	- 90º
Near-Field		
max(d)	1.047	1.043
min(d)	1.038	1.037
std(d)	0.002	0.002
Medium Field		
max(d)	1.114	NA
min(d)	1.113	NA
std(d)	0.000	NA

TABLE II
ERRORS FOR ROTATING SCANNER

statistic/rotating	Not corrected	corrected
Near-Field		
max(d)	1.210	1.170
min(d)	1.083	1.067
std(d)	0.027	0.023
Medium Field		
max(d)	1.272	1.255
min(d)	1.117	1.093
std(d)	0.037	0.034

In Fig. 11 and Fig. 12 are presented the empirical distributions for the near-field and medium field, respectively, for data collected when the scanner is rotating.

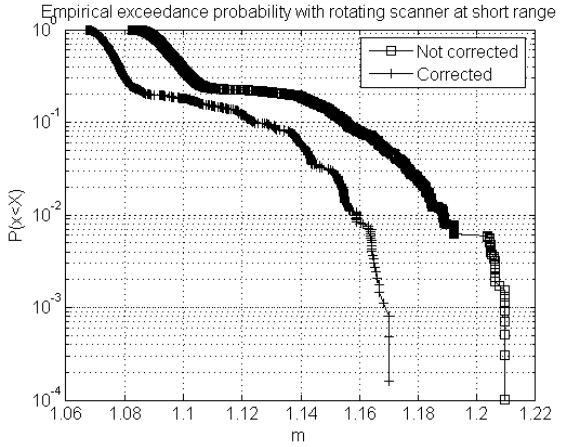

Fig. 11 Empirical exceedance distribution for short range, for real data collected when rotating the scanner.

By looking at equation (1), with an arbitrary range, the disparate amplitude of the errors can be explained as well as the form of the probability distributions. Taking $y = r\cos(\theta)\sin(\phi)$, the first aspect is that at close range the range finder has greater timing errors at short distances. Secondly, by designating the errors in ϕ as $\delta\phi$, with the probability density function $p_{\delta\phi}$, y may be rewritten as $y = r\cos(\theta)\sin(\phi_{real} + \delta\phi)$ and by applying the transformation of random variables,

$$p_{\delta\phi}|d\delta\phi| = p_y|dy| \Rightarrow p_y = p_{\delta\phi}\left|\frac{d\delta\phi}{dy}\right|, \quad (3)$$

and the law for the derivative of the inverse, one finds that y has a probability density function of the following form (apart from a multiplicative factor which depends on the interval for the errors):

$$p_y \propto \frac{p_{\delta\phi}}{\sqrt{1-(y/r\cos(\theta))^2}}. \quad (4)$$

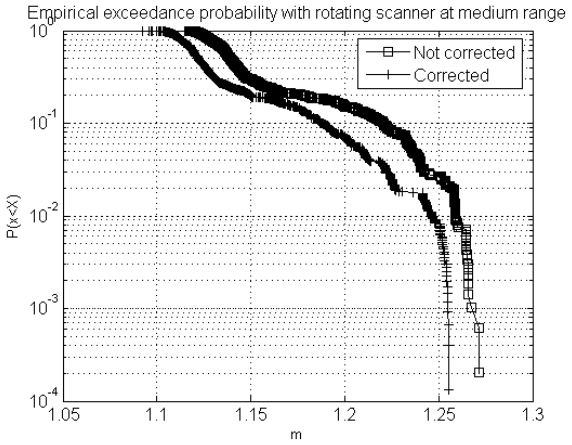

Fig. 12 Empirical exceedance distribution of distance for medium range, for real data collected when rotating the scanner.

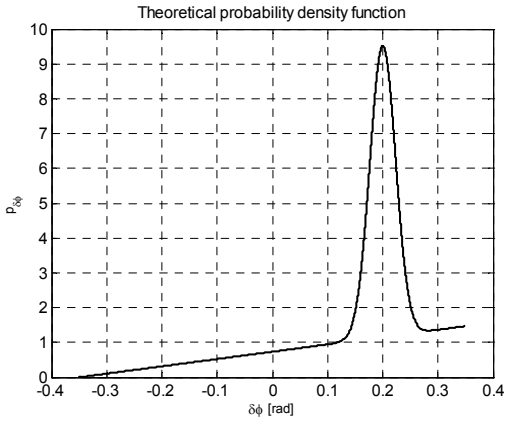

Fig. 13 The theoretical probability density function for the errors in determining the external shaft angle.

If the shape of the error probability density is chosen to be identical to that plotted in Fig. 13, which is the result of adding a truncated Gaussian added to a triangular (the approximate form may be found by a probability density estimator but here it was performed heuristically), and with the real angle taken to be $\pi/2 + \pi/10$ (just for the sake of

having a shift about the value of 1 meter obtained at $\pi/2$), then the theoretical cumulative exceedance distribution is that provided in Fig. 14. There is some resemblance to the previous figures with real data, indicating that corrections are indeed necessary and furthermore that the correction proposed herein, though important, is by itself still not enough to compensate for the errors from lack of synchronicity and possible errors in calibration of the readings from the encoder. These results indicate that it is also important to have a reference plane to estimate the lead/lag of the external angle.

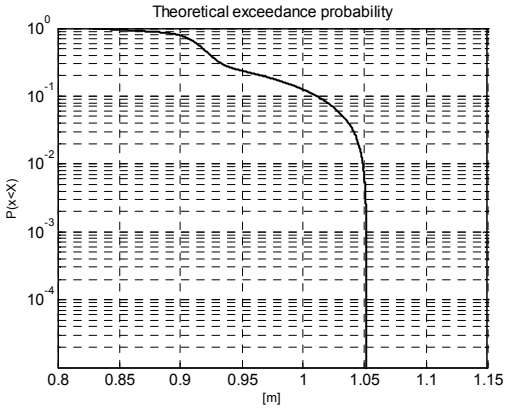

Fig. 14 Shape of the theoretical empirical distribution.

V. CONCLUSIONS

Errors due to ego-motion of 2D laser scanners, recently considered a viable solution for real-time 3D scanning, have to some extent been overlooked.

The theoretical results, backed by the results from real experimental data, have clearly demonstrated that the data from a rotating or nodding setup requires corrections if the angular rates are increased above certain levels. Even at low angular rates, and distances such as the ones associated to the real experiment reported herein, errors due to rotation reach several centimeters.

Ideally, the setup would have been to locate a long box shape on the ceiling, and to demonstrate that attributing a single external angle to the 2D scan originates wrong coordinates to an extent which cannot be overlooked. However, such was not possible at this time because it requires much more control over the experiment.

Future work will be dedicated to identifying and removing further sources of error which are triggered by the use of the range finder in dynamic environments, including additional angular and linear ego-motion due to mounting on mobile platforms.

REFERENCES

[1] Broten, G., Collier, J., 2006, "Continuous Motion, Outdoor, 2-1/2D Grid Map Generation using an Inexpensive Nodding 2D Laser Rangefinder",

[2] Nüchter, A., Lingemann, K., Hertzberg, J., Surmann, H., 2005, "Accurate object localization in 3D Laser range scans", Proc. of the 12th Intl. Conf. on Advanced Robotics. ICAR '05, 18-20 July, Seattle, WA, USA.

[3] Jiménez, A.R., Ceres, R., Seco, F., 2004, "A Laser Range-Finder Scanner System for Precise Maneouvre and Obstacle Avoidance in Maritime and Inland Navigation", Proceedings of 46th International Symposium Electronics in Marine, 16-18 June, Zadar Croatia.

[4] Jiménez, A.R., Ceres, R., Seco, F., 2009, "A Short-Range Ship Navigation System Based on Ladar Imaging and Target Tracking for Improved Safety and Efficiency", IEEE Transaction on Intelligent Transportation Systems, 10(1), pp. 186-197.

[5] Marino, R.M., Davis, W.R., 2005, "Jigsaw: A foliage-penetrating 3D imaging laser radar system", Lincoln Laboratory Journal, 15(1), pp. 23-36.

[6] SICK, Industrial Safety Systems – Safety Laser Scanners for Increased Dynamism and Efficiency.

[7] Rebai, K.; Benabderrahmane, A.; Azouaoui, O.; Ouadah, N., 2009, "Moving Obstacles Detection and Tracking with Laser Range Finder", Proc. of the 16th Intl. Conf. on Advanced Robotics, ICAR 2009, 22-26 June, Munich, Germany.

[8] Darms, M., Rybski, P., Urmson, C., 2009, "Obstacle detection and tracking for urban challenge", IEEE Transactions on Intelligent Transportation systems, 10(3), September, pp. 475-485.

[9] Himmelsbach, M., A. Müller, A., Lüttel, T., and H.-J. Wünsche, 2008, "LIDAR-based 3D Object Perception", Proc. of 1st Intl. Work-shop on Cognition for Technical Systems, München, Oct. 2008.

[10] Moosmann, F., Pink, O., and Stiller, C., 2009, "Segmentation of 3D Lidar Data in non-flat Urban Environments using a Local Convexity Criterion", In Proc. of the IEEE Intelligent Vehicles Symposium, Seiten, 215-220, Xi'an, China, June 2009.

[11] Surmann, H., Lingemann, K., Nüchter, A., Hertzberg, J., 2001, "A 3D Laser Range Finder for Autonomous Mobile Robots", Proc. of the 32nd Intl. Symp. on Robotics, pp. 153-158, Seoul, Korea, April 2001.

[12] Dias P., Matos M., Santos V., 2006, "3D Reconstruction of Real World Scenes Using a Low-Cost 3D Range Scanner". Computer-Aided Civil and Infrastructure Engineering, 21(7), October 2006, pp. s486-497.

[13] Dias P., Campos G., Santos V., Casaleiro R., Seco R., Sousa Santos B. "3D Reconstruction and Auralization of the "Painted Dolmen" of Antelas". In Proceedings of the Electronic Imaging 2008 conference, SPIE Vol. 6805, 6805OY, Three-Dimensional Image Capture and Applications 2008, San Jose, California, USA. 28-29 January 2008.

[14] Zhang, A., Hu, S., Chen, Y., Liu, H., Yang, F., Liu, 2008, "Fast Continuous 360 Degree Color 3d Laser Scanner", Intl. Archives of Photogrammetry, Remote Sensing and Spatial Information Sciences, Vol XXXVII, Beijing.

[15] CARMEN team, http://carmen.sourceforge.net/, last visited on 23rd November 2009.

[16] Simmons, R., James, D., 2001, Inter-Process Communication, Carnegie Mellon University.

[17] M. Oliveira, P. Stein, J. Almeida, V. Santos, 2009, "Modular Scalable Architecture for the Navigation of the ATLAS Autonomous Robots " 9th Conference on Autonomous Robot Systems and Competitions, Castelo Branco, Portugal, May the 7th.

[18] http://www.hizook.com/blog/2008/12/15/sick-laser-rangefinder-lidar-disassembled. Last visited on the 5th of January 2010.

[19] Lee, Sangwoo, 2006, Iterative reconstruction methods for rosette trajectories in functional MRI, PhD thesis, Electrical Eng. And Computer Science, the University of Michigan.

[20] Rahimi, E., Shokouhi, S.B., Sadr, A., 2007, "A Parallelized and pipelined datapath to implement ISODATA algorithm for rosette scan images on a reconfigurable hardware.", IEEE International Conference on Granular Computing, 2-4, pp. 433-.

[21] Dinaki, H.E., Shokouhi, S.B., Soltanizadeh, H., 2008,"Recognition of the real target in the rosette pattern using blind source separation and hidden Markov model", Proc. of the IAJC-IJME Intl. Conf., 17-19 November, Nashvile, Tennessee, USA.

[22] DiMarco, J.S., Kemper, P.J., Pringle, L.N., 1999, "Closed loop guidance of imaging infrared missile seekers", Proc. SPIE Conference on Infrared Imaging Systems: Design, Analysis, Modeling and Testing,, vol. 3701, pp. 254-265, Orlando Florida, USA, April.

[23] SICK, 2006, LMS200/211/221/291 Laser Measurement Systems – Technical Description. Document 8008970/QI72/2006-12.